

Article

Experimental Evaluation on Engineering Properties and Drying Shrinkage of No-Cement Mortar Produced by Alkaline Activation of Fly Ash-Slag Mixtures

Thi Hai Yen Nguyen^{1,a}, Nguyen Thi Cao^{2,b}, Tran Dong Minh Ngoc^{3,c},
and Trong-Phuoc Huynh^{4,d,*}

¹ Department of Civil Engineering, Industrial University of Ho Chi Minh City, 12 Nguyen Van Bao Street, Ward 4, Go Vap District, Ho Chi Minh City 70000, Vietnam

² Department of Civil Engineering, Faculty of Engineering, Tien Giang University, 119 Ap Bac Street, Ward 5, My Tho City, Tien Giang Province 84000, Vietnam

³ School of Graduate, Can Tho University, Campus II, 3/2 street, Ninh Kieu District, Can Tho City 94000, Vietnam

⁴ Department of Civil Engineering, College of Engineering Technology, Can Tho University, Campus II, 3/2 street, Ninh Kieu District, Can Tho City 94000, Vietnam

E-mail: ^anguyenthihaiyen@iuh.edu.vn, ^bcaonguyenthi@tgu.edu.vn, ^cngocm4218013@gstudent.ctu.edu.vn, ^{d,*}htphuoc@ctu.edu.vn (Corresponding author)

Abstract. Turning locally available industrial by-products such as fly ash (FA) and ground granulated blast-furnace slag (GGBFS) into cement-free materials has been recently received much attention from researchers. Following this trend, the present study produces alkali-activated mortars (AAFS) using a mixture of FA and GGBFS as a precursor activated by an alkaline solution of sodium hydroxide and sodium silicate. Five AAFS mixtures were prepared for the evaluation of engineering properties, drying shrinkage, and microstructural observation using various FA/GGBFS ratios of 30/70, 40/60, 50/50, 60/40, and 70/30. The experimental results show that the proportions of FA and GGBFS significantly affected the performance of the AAFS in both fresh and hardened stages. Higher GGBFS content resulted in a reduction in flowability and higher fresh unit weight. The GGBFS-rich AAFS developed its mechanical strength faster than the FA-rich AAFS and the strength gain of the GGBFS-rich AAFS was significantly higher than that of the cement-based mortar at only 1-day old, confirming the applicability of AAFS as a structural material and its potential to replace cement in the no-cement mortar production. The AAFS sample incorporating 60% of GGBFS and 40% of FA exhibited the highest strength, lowest water absorption, and less drying shrinkage with a relatively dense microstructure among the AAFS samples.

Keywords: Alkali-activated mortar, fly ash, ground granulated blast-furnace slag, drying shrinkage, microstructure.

ENGINEERING JOURNAL Volume 26 Issue 3

Received 9 December 2021

Accepted 9 March 2022

Published 31 March 2022

Online at <https://engj.org/>

DOI:10.4186/ej.2022.26.3.17

1. Introduction

Fly ash (FA) and ground granulated blast-furnace slag (GGBFS) are by-products that have been regarded as problematic solid waste in many countries. FA is a by-product of coal-based thermal power plants. Therefore, the recent increase in power demand will lead to a higher quantity of released FA. For instance, about 120 – 150 million tons of coal FA is annually generated in India, the largest FA-produced country, and about 100 million tons in China each year [1]. In developing countries such as Vietnam, a member of ASEAN (Association of Southeast Asian Nations), at least 23 coal-fired power plants are currently operating commercially and the total amount of generated FA is around 12.2 billion tons per year [2]. So far, coal has been considered as an optimum power generation fuel for ASEAN countries in terms of both cost and energy security [3]. In recent years, the use of FA in various applications has been investigated. For example, the inclusion of 15 – 20% FA in deep cement mixing columns was suitable for embankment support [4, 5]. Another study found that about 10% FA was suitably used in combination with ordinary Portland cement (OPC) and dredged sediment to enhance the properties of materials prepared for road application [6]. Moreover, Adamu et al. [7] stated that the use of high volume FA (0 – 80%) in concrete may not only help to reduce cost and improve ultimate strength but also promote the environmental sustainability. Besides, GGBFS is also a by-product of the manufacture of pig iron in the blast furnace that affects the environmental sustainability problem. It is noted that the amount of both FA and GGBFS is increasing yearly and this poses a significant challenge for environmental protection in developing countries.

Utilizing industrial solid by-products as an alternative to OPC in the concrete and cement industry has been recognized as one of the sufficient methods to solve these wastes. The processes of OPC production consume a significant amount of natural resources (i.e., lime, clay, etc.) and release a large volume of CO₂ [8]. Therefore, there have been some promising techniques for researchers over the world to create a new type of binder that can replace OPC in concrete by using FA and GGBFS to develop a kind of green construction material. In recent years, alkali-activated binders have emerged as an environmentally friendly material alternative to OPC [8]. Alkali-activated materials (AAM) can be designed from by-products, largely based on GGBFS and FA because of their relatively low cost and sufficient compositions [9]. In this way, AAM can be separated into two individual systems [10], including a high calcium system and a low calcium system, which is also known as alkali-activated slag (AAS) and alkali-activated fly ash (AAF), respectively. Besides, the normally used alkaline solution is a mixture of sodium silicate (SS) and sodium hydroxide (SH) solutions [8]. However, there are some drawbacks to these two systems. Regarding AAS, it has a problem of quick setting because the dissolution of aluminosilicates from GGBFS promotes the rapid setting [9]. Meanwhile, a number of

previous research [11, 12] reported that AAF pastes and concrete had good mechanical and durability properties when they were cured at elevated temperatures (i.e., 60 – 85°C) to gain early-age strengths [13], whilst the reactivity of FA at the ambient temperature is too low to be activated by alkali activators [14]. This is not appropriate for cast-in-situ concrete in practice. Therefore, it is essential to find a new AAM system that can attain engineering properties under ambient curing conditions. Hence, a combination of GGBFS and FA has emerged to create an alkali-activated FA-GGBFS blended system (AAFS). Binary FA-GGBFS mixtures can be able to control the setting time and hardening of the blend at an early age [15]. Moreover, the addition of GGBFS can accelerate FA dissolution and increase reaction product formation under ambient curing conditions.

Prior studies which investigated the mechanical properties of AAFS mortars with different FA/GGBFS ratios of 50/50, 30/70, and 0/100 showed that higher compressive and flexural strengths of AAFS mortars were attained compared to OPC mortars [16]. It was also suggested that the FA/GGBFS ratio of 50/50 activated by 6% of Na₂O (by weight of cementitious material) was optimal for making AAFS. Besides, Abdelilah et al. [9] indicated that the short-term strength of AAFS grout was primarily provided by the reactivity of GGBFS, and the maximum strength was observed with the inclusion of 20 – 40% of FA. The effect of SS/SH ratios on the compressive strength of AAFS mortars was also evaluated in an experimental study conducted by Alanazi et al. [8] when 10% and 15% of GGBFS were used as an additive. The authors concluded that mixtures with an SS/SH ratio of 1.0 generally exhibited higher compressive strength than those with an SS/SH ratio of 2.5.

Besides, drying shrinkage is an important parameter influencing the durability of the material. The drying shrinkage of AAFS mortars can be observed based on their length changes. Chi et al. [16] reported that AAFS mortars showed a higher length change than OPC mortars and an increasing amount of FA led to a lower rate of length changes of AAFS mortars. In addition, the shrinkage characteristics of AAFS mortars were investigated in the study by Lee et al. [17]. The data from the drying shrinkage test showed that most of the total drying shrinkage took place during the first day and was nearly identical to the 2nd to the 28th day. Moreover, the FA/GGBFS ratio had a significant influence on the drying shrinkage rate of AAFS mortars whereby the addition of FA could reduce the drying shrinkage rate [18]. There was also an influence on the drying shrinkage of AAFS mortars from the liquid/binder (L/B) ratio. AAFS mortars with the L/B ratio of 0.5 showed a decrease in drying shrinkage values in comparison with mortars prepared with the L/B ratio of 0.6 [18].

In general, the number of studies related to this binary material system is still relatively limited [9], especially in terms of drying shrinkage, which might be more complex than those of AAF or AAS [17]. Besides, the starting precursor materials used in various studies were diverse,

making the results obtained in different studies also incomparable. It is fact that the characteristics of starting materials greatly influenced the performance of the resultant materials. Therefore, the present study carries out experiments to evaluate mechanical properties of AAFS mortars such as compressive strength, flexural strength and especially drying shrinkage since it controls the cracking generation. Moreover, the performances of AAFS regarding drying shrinkage behavior and early mechanical strength at ambient curing conditions are evaluated to clarify the adaption of using as structural building material replacing OPC-based materials (i.e., mortars, concrete, etc.). To prepare the AAFS samples, local sources of FA and GGBFS are utilized in different proportions (0 – 100%) and a solution of SH and SS is used as an alkaline activator. In this study, blended crushed sand and river sand are used as fine aggregates in the AAFS mixtures. The AAFS mortar samples are tested for both fresh (i.e., flowability and unit weight [UW]) and hardened properties (i.e., flexural strength, compressive strength, water absorption, and drying shrinkage). Moreover, the microstructures of the AAFS mortars are characterized using scanning electron microscopy (SEM) analyses. This study further provides a positively sufficient solution of industrial solid by-products (i.e., FA and GGBFS) treatment and the production of more environmentally friendly materials to alternate the use of conventional OPC-based materials in green and sustainable construction.

2. Materials and Experimental Methods

2.1. Materials

In this study, the AAFS samples were prepared using a mixture of FA (specific gravity of 2.14) and GGBFS (specific gravity of 2.85) as a precursor, a solution of SH and SS as an alkaline activator, and blended crushed sand and river sand as fine aggregate. All of these materials (Fig. 1) are locally available. The chemical compositions of FA and GGBFS are given in Table 1. It can be seen that FA comprises mainly of SiO_2 and Al_2O_3 while SiO_2 , Al_2O_3 , and CaO are the major components of GGBFS. These chemical elements play a crucial role in the alkaline activation process [19, 20]. The alkaline activator was prepared using SH of 5M (made from NaOH flake of 98% purity) and SS liquid (solid contents of 25.72% SiO_2 and 8.63% Na_2O). Figure 2 shows the SEM micrographs of FA and GGBFS used in this research. It can be seen that FA contains mainly spherical beads with crust glassy surface and the particle size ranging mostly about 7-28 μm . Meanwhile, the GGBFS includes crushed particles with an average size of approximately 5 μm .

Besides, to obtain a good gradation of fine aggregates for making AAFS samples as shown in Fig. 3, blended crushed sand (35 wt.%) and river sand (65 wt.%) are suggested based on the preliminary trials. It is noted that the density, water absorption, and fineness modulus of crushed sand are 2840 kg/m^3 , 0.82%, and 3.05,

respectively. Whereas, the corresponding values for river sand are 2670 kg/m^3 , 0.62%, and 1.58. Besides, local brand OPC with a specific gravity of 2.93 is used to prepare the control mortar in this study.

Table 1. Chemical compositions of FA and GGBFS.

Materials	FA	GGBFS
SiO_2	59.2	35.9
Al_2O_3	26.7	13.0
Fe_2O_3	6.1	0.3
MgO	0.9	7.9
CaO	1.1	38.1
Others	6.0	4.8

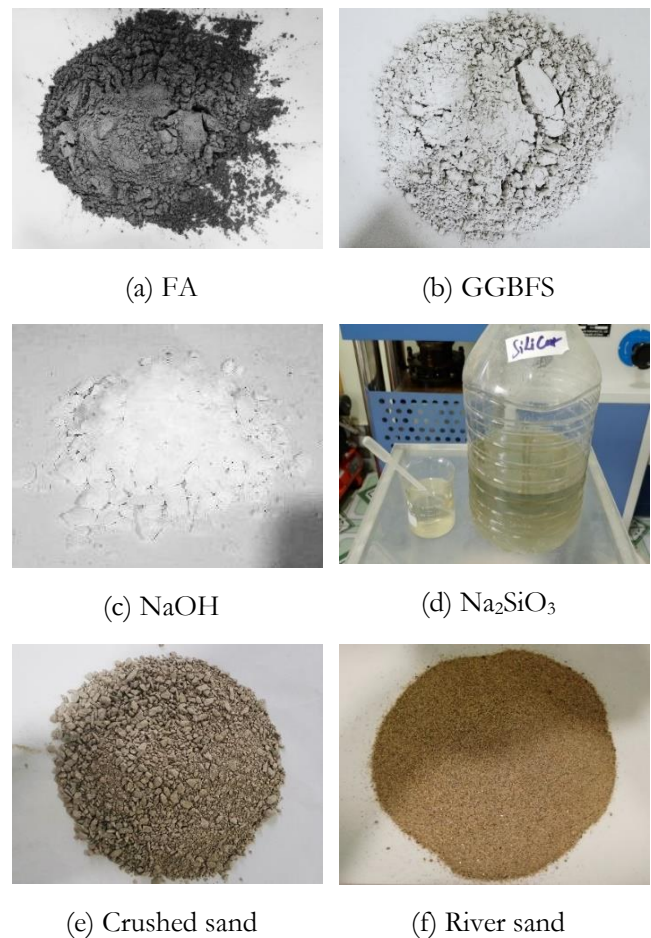


Fig. 1. Raw materials used for preparing AAFS samples.

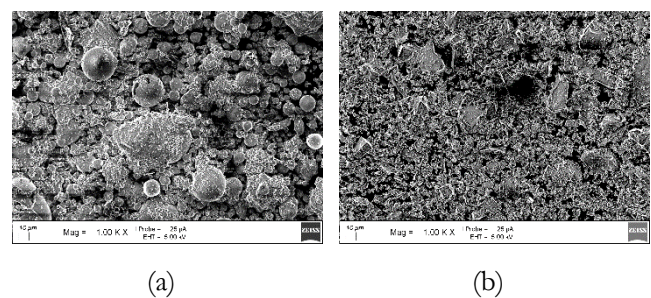


Fig. 2. SEM images of (a) FA and (b) GGBFS particles.

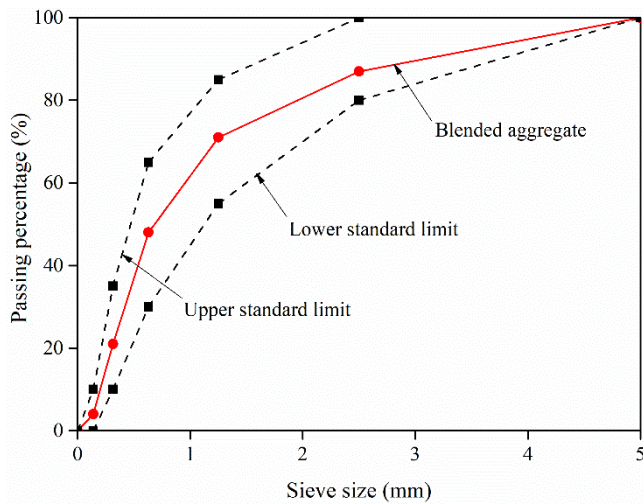


Fig. 3. Particle size distribution of blended aggregates.

2.2. Mixture Proportions

The mixture proportions of the AAFS samples were calculated following the procedures as previously described by Huynh et al. [21]. In which, this study used the alkali equivalent (AE, the weight ratio of Na_2O /total cementitious materials), alkali modulus (M_s , the molar ratio of $\text{SiO}_2/\text{Na}_2\text{O}$), and the liquid-to-solid (L/S) ratio of 5%, 0.8, and 0.42, respectively. It is noted that liquid (L) includes mixing water and water in both SH and SS solutions. Meanwhile, solid (S) includes FA, GGBFS, and solid parts in both SH (Na_2O) and SS (Na_2O and SiO_2) solutions. In addition, the ratio of fine aggregates/binders (including FA and GGBFS) was fixed at 2.5 for all AAFS mixtures. Hence, the proportion of each material used for the preparation of AAFS samples was calculated as shown in Table 2. For comparison purposes, the OPC mortars (C100 mix) were also prepared in this study with the amount of OPC, water, crushed sand, and river sand of 559.1, 306.1, 489.2, and 908.5 kg/m^3 respectively.

Specifically, the procedures for calculating material proportions are briefly described as follows: It is assumed that the total amount of needed FA and GGBFS to prepare the AAFS samples used for the experiment is 7500 g. Based on the results of pre-trials in the laboratory, the designed parameters are fixed at $\text{AE} = 5\%$, $M_s = 0.8$, and $L/S = 0.42$. The used 5M SH has Na_2O content of 15.3% and SS has 25.72% of SiO_2 and 8.63% of Na_2O .

Step 1. Determine total weight of Na_2O

$$\text{AE} = \frac{\text{Na}_2\text{O}}{(\text{FA} + \text{GGBFS})} \quad (1)$$

$$\rightarrow \text{Na}_2\text{O} = 5\% \times 7500 = 375 \text{ g}$$

Step 2. Determine the amount of SS solution

$$M_s = \frac{\text{SiO}_2}{\text{Na}_2\text{O}} \Leftrightarrow \frac{(25.72\% \times \text{SS}) / 60.09}{(375 / 61.98)} = 0.8 \quad (2)$$

$$\rightarrow \text{SS} = 1131 \text{ g}$$

Step 3. Determine the amount of SH solution

$$\text{Na}_2\text{O} = (15.3\% \times \text{SH}) + (8.63\% \times \text{SS})$$

$$\Leftrightarrow 375 = (0.153 \times \text{SH}) + (0.0863 \times 1131) \quad (3)$$

$$\rightarrow \text{SH} = 1813 \text{ g}$$

Step 4. Determine the amount of mixing water (W)

$$\frac{L}{S} = \frac{W + W_{\text{in SH}} + W_{\text{in SS}}}{(\text{FA} + \text{GGBFS}) + \text{Na}_2\text{O}_{\text{in SH}} + (\text{Na}_2\text{O} + \text{SiO}_2)_{\text{in SS}}}$$

$$\Leftrightarrow 0.42 = \frac{W + 1813(1 - 0.153) + 1131(1 - 0.2572 - 0.0863)}{7500 + (1813 \times 0.153) + 1131(0.2572 + 0.0863)} \quad (4)$$

$$\rightarrow W = 1172 \text{ g}$$

Step 5. Determine the content of fine aggregates

$$\frac{[\text{River sand (65\%)} + \text{Crushed sand (35\%)})]{\text{FA} + \text{GGBFS}} = 2.5 \quad (5)$$

$$\rightarrow \begin{cases} \text{River sand} = 0.65 \times 2.5 \times 7500 = 12188 \text{ g} \\ \text{Crushed sand} = 0.35 \times 2.5 \times 7500 = 6563 \text{ g} \end{cases}$$

Table 2. Mixture proportions of AAFS samples (kg/m^3).

Mixtures	F3S7	F4S6	F5S5	F6S4	F7S3
FA	171.5	227.1	282.1	336.3	389.8
GGBFS	400.1	340.7	282.1	224.2	167.0
NaOH	138.2	137.3	136.4	135.5	134.6
Na_2SiO_3	86.2	85.6	85.1	84.5	84.0
Water	89.3	88.7	88.2	87.6	87.0
River sand	928.9	922.8	916.7	910.7	904.8
Crushed sand	500.2	496.9	493.6	490.4	487.2

The calculated values are then converted to obtain the weight of materials that are equivalent to the total volume of exactly one m^3 as tabulated in Table 2 based on the specific gravity or density of each material.

2.3. Sample Preparation

To make the AAFS samples for the experiments, all of the raw materials were firstly prepared based on the proportions as shown in Table 2. FA and GGBFS were dry mixed in for 1 min then the alkaline solution was gradually added to the dry mixture which was mixed continuously for 3 mins to obtain a homogeneous paste. Next, fine aggregates were added to the mixer followed by mixing water. The mixer was allowed to run for an additional 3 mins to obtain a uniform mixture. Right after that, the fresh mixture was tested for flowability and UW, and the mortar samples were finally casted in the molds with different dimensions for various test methods as described in the next section. All of the samples were de-molded 24 hours after casting and then cured in the laboratory at a temperature of $27 \pm 2^\circ\text{C}$, relative humidity of $65 \pm 5\%$ until testing.

2.4. Test Methods

The fresh AAFS and C100 mixtures were checked for flowability and unit weight right after mixing following the

procedures described in ASTM C1437 and ASTM C138, respectively. In addition, the flexural and compressive strengths of the hardened samples were tested under a modified version of ASTM C348 and ASTM C349, respectively. These tests were conducted at the sample ages of 1, 7, and 28 days using prismatic samples of $40 \times 40 \times 160$ mm. The water absorption of the hardened mortars was measured at 28 days of age using the samples in dimensions of $50 \times 50 \times 50$ mm following the ASTM C1403. Whereas, the drying shrinkage of the mortars was monitored at 0, 1, 7, 14, and 28 days in accordance with ASTM C490 using the samples with dimensions of $25 \times 25 \times 285$ mm. Besides, the SEM observation was performed at 28 days using the broken pieces collected after the compression test. It is noted that the collected pieces were soaked in methyl alcohol to stop further hydration before the SEM observation and the procedures for preparing the test samples used in this study were similar to that reported by Hwang et al. [22].



Fig. 4. Apparatus for testing properties of the AAFS.

3. Results and Discussion

3.1. Flowability and Fresh UW

The flowability of the AAFS mortars in this study was evaluated by measuring the flow diameter of the fresh mixtures with the results as shown in Fig. 5. It can be observed that the lowest flow diameter value (180 mm) was measured at the F3S7 mixture, which contained the highest GGBFS content (70%). Meanwhile, the F7S3 mixture with the lowest content of GGBFS (30%) attained the highest flow diameter value of 240 mm. Figure 5 shows that the flow diameter values decrease with the increase of GGBFS content, which is consistent with previous research [14, 23]. This can be attributed to an arrangement of the particles, particularly the angular shape of GGBFS in comparison with the spherical shape of FA particles. The free flow of the mortar was encouraged due to the spherical shape of FA particles while the angular GGBFS particles prevent the flow as a result of higher interlocking between particles [15].

It should be noticed that the alkali solution can become more viscous due to the faster dissolution of aluminosilicates of GGBFS [15]. Except for the F3S7 mixture, flow diameter values of the AAFS mixtures were higher than those of the control mixture using OPC. Besides, the fresh UW values of the mortar mixtures were also presented in Fig. 5. The highest fresh UW value of 2262 kg/m^3 was observed in the case of the control mixture. Whereas all of the AAFS mixtures registered lower fresh UW values than that of the OPC mixture. Indeed, the AAFS mixtures with various proportions of FA and GGBFS had fresh UW values in the ranges of $2222 - 2245 \text{ kg/m}^3$. This result is due to the lower specific gravities of both FA and GGBFS compared to those of OPC. On the other hand, the fresh UW values of the AAFS mixtures were found to reduce by lowering the GGBFS content (or increasing the FA content) in the mixtures because FA had lower specific gravity than GGBFS (see Table 1). As a result, the lowest fresh UW value was observed for the AAFS containing 70% of FA and 30% of GGBFS. Thus, the inclusion of more FA in the AAFS was beneficial in terms of flowability and fresh UW of the mortar mixtures.

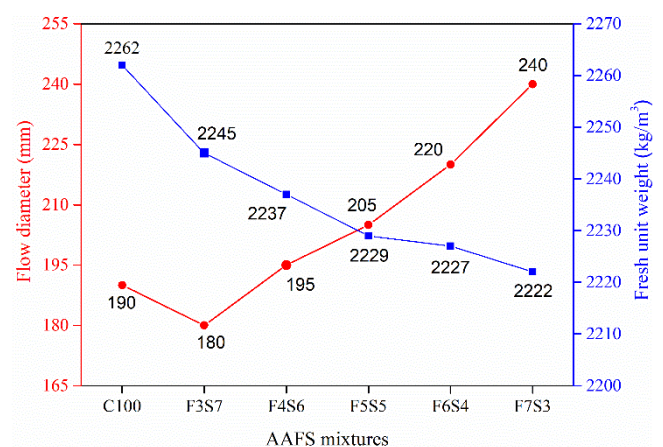


Fig. 5. Flowability and UW of fresh AAFS mixtures.

3.2. Flexural Strength

The flexural strength is one of the most important parameters, particularly in the early ages of the mortars. It determines the potential to apply the mortars widely as a structural material. In this study, the flexural strength values of the AAFS samples were measured with the results as presented in Fig. 6. Overall, AAFS samples expressed higher flexural strength than that of the OPC sample (C100 mix) except for the mixture with high FA content ($\geq 50\%$) at 1 day. Though the superior rate of the flexural strength of AAFS mortar strongly depended upon the composition of the AAFS binder, it once again emphasizes the ability to use the alkali-activated binders to replace OPC in the production of mortars. In detail, the F3S7 and F4S6 samples showed meaningful higher flexural strength than that of the C100 sample at all curing ages considered in this research. For the F3S7 sample, the 1-day flexural strength was approximately 43% higher than that of the control sample while it was about 22% and 35% higher than the flexural strength values of the C100 sample at 7 and 28 days, respectively. Meanwhile, the flexural strength of the F4S6 sample was about 32%, 29%, and 39% higher than that of the C100 sample at the ages of 1, 7, and 28 days, respectively. Nevertheless, the F5S5, F6S4, and F7S3 samples gained flexural strength values of approximately 18, 32, and 59% lower than that of the C100 sample at 1 day, respectively. However, the flexural strength of these AAS mortars evolved significantly in the following days and then overcame the flexural strength of the C100 after 7 days. At this age, the F5S5, S6S4, and S7F3 samples registered flexural strength values of about 18, 12, and 3% higher than that of the C100, respectively. These flexural strength values kept increasing further with curing time. At the age of 28 days, the flexural strength values of the F5S5, F6S4, and F7S3 samples reached 7.99, 7.54, and 6.63 MPa, which were about 24, 17, and 3% higher than that of C100 at the same age.

Furthermore, it is found that the flexural strength gains of AAFS mortars varied differently depending on the GGBFS content and the curing age. At 7 days, the flexural strength of the samples containing 50, 60, and 70% FA grew quickly where they were about 87, 113, and 213% higher than that at 1 day. The rate of strength increment became slower after 7 days. For instance, the flexural strength values at 28 days of the AAFS mortars with 50 – 70% FA were only about 10 – 15% higher than that at 7 days. Nevertheless, the evolution of the flexural strength of samples containing 30% and 40% FA (or 60% and 70% GGBFS) from 1 to 7 days and 7 to 28 days was more consistent, about 10 – 25%. The activation of FA in alkaline solution is a time-consuming process, leading to a low strength gain of FA-based geopolymer at an early age [24]. Therefore, the evolution of flexural strength of AAFS mortars at 1 day was mainly thanks to the hydration of GGBFS [25]. Consequently, at 1 day, higher GGBFS content resulted in the higher flexural strength of the AAFS mortars and the strength gap between the GGBFS-poor and the GGBFS-rich samples was significant.

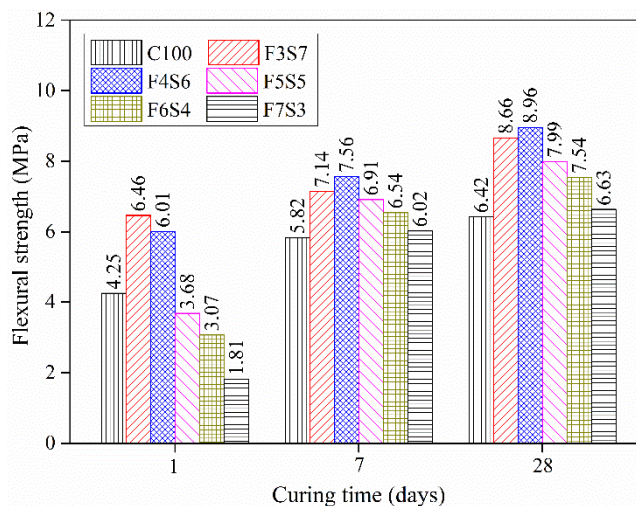


Fig. 6. Flexural strength of AAM samples.

Indeed, the F3S7 sample obtained the highest flexural strength value of 6.46 MPa, which was about 3.6 times higher than that of the F7S3 samples with the lowest flexural strength value of 1.81 MPa. However, FA was activated and partly dissolved later on [26]. The polymerization of dissolved species from FA helped the AAFS samples gain strength and attributed to the lessening of the strength gap between the high- and low-GGBFS samples. The strength gap was only 25% and 35% between the highest (F4S6) and the lowest (F7S3) flexural strength at 7 and 28 days, respectively.

Notably, in this study, the flexural strength values of the F3S7 and F4S6 AAFS mortars were higher than those of the C100 at all curing ages and their flexural strengths at 1 day were about 67 – 74% of those at 28 days. The rapid evolution of strengths at the early age of the AAFS mortars brings out great advantages in terms of its applicability in the construction industry. As is well-known, turning over the scaffolding and formwork on the construction site as quickly as possible is the key to save the construction cost. To do that, the used materials need to reach their design strengths as fast as possible without causing severe defects in macroscale as well as microscale, which determines the long-term performance of the structure. Mortar samples of F3S7 and F4S6 initially exhibited the adaptable flexural strength of structural material.

3.3. Compressive Strength

The evolution of compressive strength of the control and AAFS mortars at various ages is presented in Fig. 7. A similar trend observed on the flexural strength was obtained here, where the compressive strength of the samples increased with the increase of GGBFS from 30 to 60% and reversed after that. Remarkably, the compressive strength of all AAFS mortars was higher than that of the control specimen at all curing ages considered here, except the sample with 70% FA at 1 day.

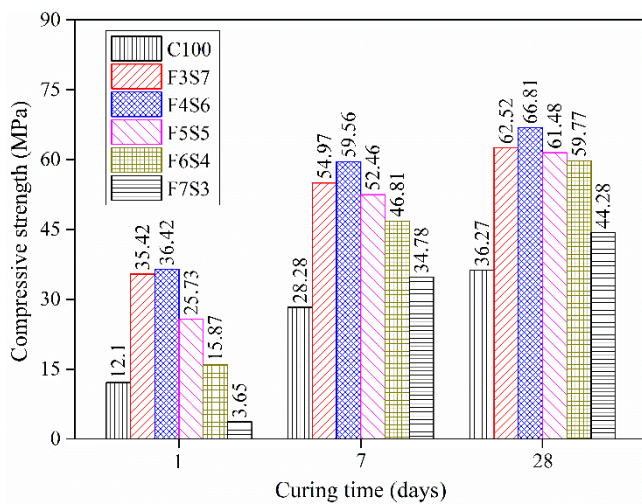


Fig. 7. Compressive strength of AAFS samples.

In detail, at 1 day, the compressive strength of the F3S7 and F4S6 was approximately 3 times higher than that of the control sample and about 2.1 times for the F5S5 sample. Similarly, the F6S4 sample showed a higher compressive strength (about 31%) than the C100 sample. However, the F7S3 expressed a significantly lower compressive strength than that of the C100. At the later ages, though the control sample gained strength quickly, the compressive strength evolution of AAFS mortars was also meaningful, particularly the F7S3 sample, where it overcame and reached the compressive strength of about 1.2 times of the C100's compressive strength at 7 days. Meanwhile, the other AAFS mortars expressed a compressive strength of 1.6 to 2.1 times higher than that of the C100. At the age of 28 days, the AAFS mortars obtained compressive strength values of about 1.2 – 1.8 times higher than that of the C100 sample. The low strength of FA-rich AAFS is obviously due to the relatively low reactivity of spherical FA bead [27, 28], which is surrounded by the glassy, dense, and stable surface, as presented in Fig. 2.

In order to activate the FA, that glassy surface needs to be dissolved in a high pH environment, which is a time-consuming process before the inside components of FA can react [16]. Nevertheless, GGBFS is considered a type of cement. The crushed surface of GGBFS can hydrate with water well, forming C-(A)-S-H, ettringite, monosulfate, and other hydration products. Alkali solution can help to promote that hydration process to be more rapid, gaining significant strength at an early age [16]. Furthermore, as exhibited in Fig. 2, the size of GGBFS particles was smaller than that of FA. With the lower size and crushed surface, it would be easier to activate GGBFS compared to FA, resulting in higher compressive strength of GGBFS-rich AAFS mortars.

Based on the results of the flexural and compressive strengths as presented in Fig. 6 and Fig. 7, respectively, the contribution of FA activated on the evolution of strengths at an early age was very limited. However, the appropriate content of FA showed a beneficial effect since the F4S6 expressed a greater strength than that of F3S7. Previous studies indicated that micro-cracking growing in the AAS

and the micro-cracking developed over time [24, 25], leading to a lower compressive strength than AAFS mortars [25]. Apparently, before being activated, FA can be a filler densifying the micro-crack generated by the GGBFS in the mortar. In this research, 40% of FA was probably a sufficient quantity to fill the cracks and pores produced by 60% of GGBFS hydrated, resulting in the optimum strength. The high compressive strength of F3S7 and F4S6 mortar specimens explicitly confirmed the applicability of AAFS as a structural material and its potential to replace cement in the mortar/concrete industry. Furthermore, it helps to solve the waste materials from other industries as well as reduce the environmental burden.

3.4. Water Absorption

Water absorption is one of the most important factors of mortar performance. It reveals the capillary pores in the specimen and is one of the main factors used to predict the durability of mortars and reinforced concrete structures, particularly when the materials expose an aggressive environment. Figure 8 presents the water absorption of AAFS mortars and control samples at 28 days. Remarkably, the water absorption of the AAFS mortars was significantly lower than that of the control sample (C100), ranging from 13 to 32%. It is found that the increase of GGBFS content in the AAFS mixtures from 30 to 60% led to the decline of water absorption but then it reversed at 70%.

The variation of water absorption with the increase of GGBFS was in good agreement with the flexural strength and the compressive strength of the AAFS mortars as above discussion. As is well-known, the water absorption of mortars/concrete is proportional to the porosity, which is inversely proportional to the mechanical strength [29]. On FA-rich AAFS mortars, the obtained strength was relatively low, especially at the early ages. Implicitly, the porosity was significant, bringing out the high water absorption of these mortars. Nevertheless, on GGBFS-rich samples, the obtained strength was profound, which should be a consequence of samples possessing low porosity, implying samples with low water absorption. Kuo et al. [30] and Mohamed [31] also confirmed that the porosity of AAS concrete reduced as increasing the content of GGBFS in the mixture. Furthermore, the increase of water absorption of the F3S7 compared to the F4S6 was also associated with the decline of strength since GGBFS increased from 60 to 70%. Obviously, the filler effects of appropriate content of FA used and the generation of gel from the activation of FA filling the micro-crack produced by the hydration of GGBFS helped to densify the matrix of the mortars and then improve the strength as well as reduce the water absorption of AAFS mortars [24, 32].

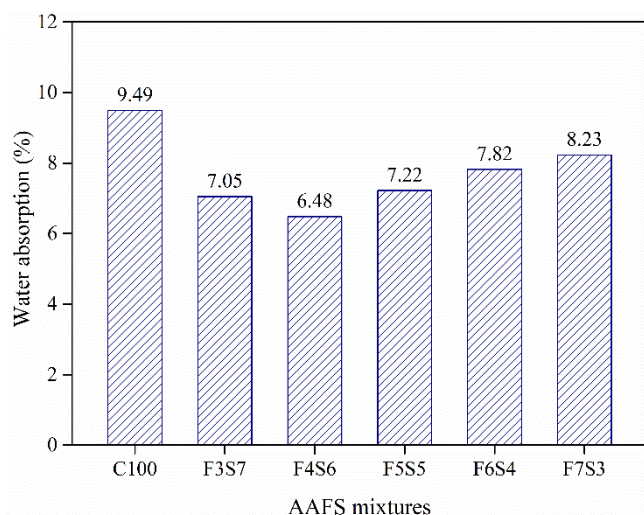


Fig. 8. Water absorption of AAFS samples.

3.5. Drying Shrinkage

Drying shrinkage is another important property of AAFS mortars that determines the ability to use AAFS mortars as a building material since it controls the cracking generation and influences the durability of the AAFS [33]. Figure 9 shows the drying shrinkage of the AAFS mortars with various proportions of FA and GGBFS. Notably, the drying shrinkage of the AAFS mortars was much more significant than that of the control sample. Furthermore, the drying shrinkage seemed stagnant after the curing time reached 14 days. Figure 9 indicates that the drying shrinkage of the AAFS mortar increased with the increase of FA. The F3S7 and F4S6 samples showed about 2 times higher drying shrinkage compared to that of the C100 while it was about 3 – 4.2 times on the others.

As being recognized, the drying shrinkage is mainly rooted in the evaporation of free water from the pore structure. Some previous studies indicated that the drying shrinkage of AAFS material was about 3 – 6 times higher than that of OPC-based material [34, 35]. However, some other research expressed contradictory results where the lower drying shrinkage of AAFS compared to OPC-based material was found [36, 37]. In this research, the drying shrinkage of the AAFS mortar was significantly higher than that of the C100. Furthermore, the increase of FA increased drying shrinkage. It is probably due to the ability of FA to refine the pore structure of AAFS mortar, which may lead to a higher mesopore volume since the FA content increased, causing a high potential of drying shrinkage [17]. In addition, another study showed that a higher drying shrinkage was found on AAFS specimens with higher physically bound water, which is determined by the microstructure of the AAFS specimen and gel formed from the AAFS binder. Implicitly, the drying shrinkage of AAFS mortars is dependent upon not only the free water and pore structure of the AAFS specimen but also the composition and microstructure of the AAFS specimen [38].

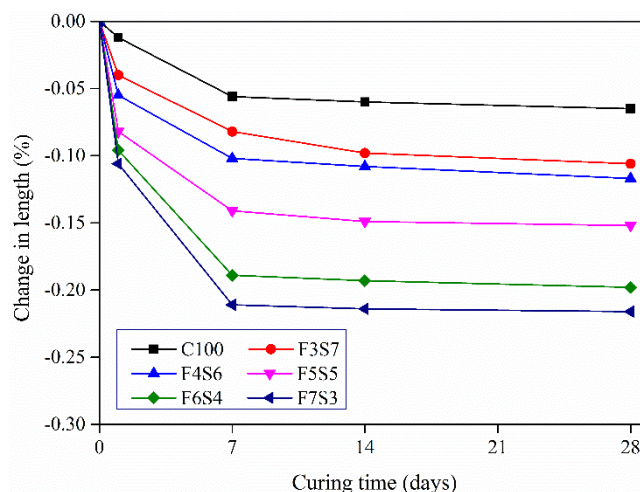


Fig. 9. Drying shrinkage of AAFS samples.

When the AAFS binder was activated, the C-A-S-H gel produced from GGBFS and N-A-S-H formed from FA coexisted [39, 40]. Note that C-(A)-S-H comprises a calcium oxide layer sandwiched between silicate chains on both sides, whereas N-A-S-H is a 3D zeolitic-like gel of the amorphous alkaline aluminosilicate. It should be mentioned here, the physically bound water of the gel strongly depends on the zeta potential of the gel which is affected by many factors including the content and valance of cations of the gel and in the pore solution. C-(A)-S-H can attract tighter water than N-A-S-H. Since the FA increased, the ratio of N-A-S-H in the gel mixture increased [39, 40]. Therefore, FA-rich AAFS revealed higher drying shrinkage than GGBFS-rich AAFS mortars.

Moreover, in the F3S7 and F4S6 samples, where the GGBFS content was high, the hydration products in the system were mainly C-(A)-S-H, portlandite, ettringite, and monosulfate. These hydration products are similar to those formed by the hydration of OPC. Therefore, it is reasonable since the GGBFS contents in the specimens increased, their drying shrinkage got close to that of the C100 specimen. Further research should be carried out in order to understand the mechanism of drying shrinkage in AAFS specimens.

3.6. SEM Observation

The SEM images of AAFS mortars with FA-to-GGBFS ratios of 30/70, 40/60, 50/50, 60/40, 70/30, and control sample at 28 days with the same magnification of 1000 times are presented in Fig. 10. In addition to the amorphous microspheres of FA, which were surrounded by the reaction products, the unreacted FA could be seen abundantly in F7S3 and F6S4 samples. Furthermore, high porous microstructures were observed with large pores. Obviously, due to the slow reaction of the high ratios of FA, the slow formation of reaction products was caused and then, resulting in the low strength as well as high water absorption. The high porous microstructure also helps water to evaporate, causing higher drying shrinkage of FA-rich AAFS mortar, as discussed above.

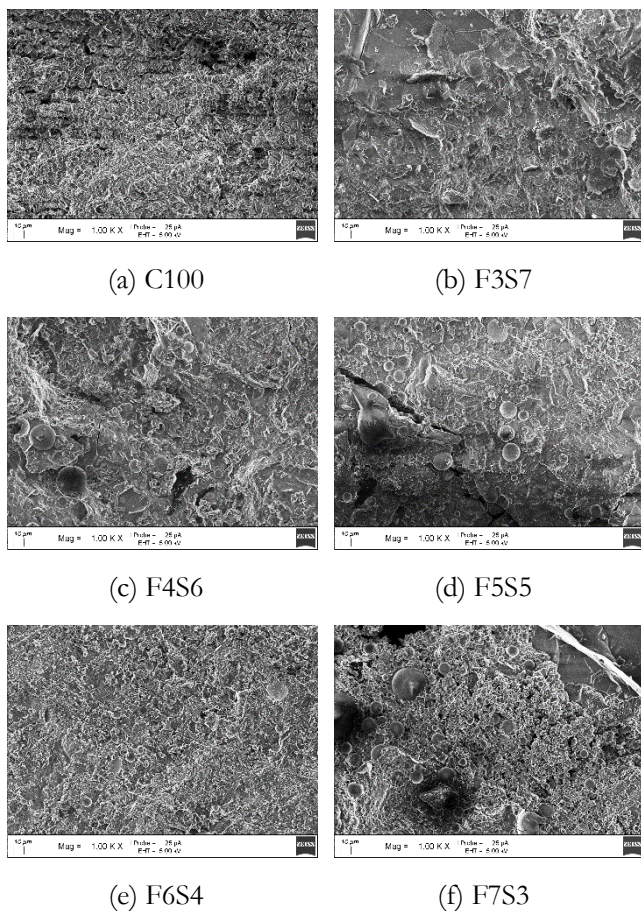


Fig. 10. SEM micrographs of AAFS samples at 28 days.

Nevertheless, the F3S7, F4S6, and F5S5 samples exhibited rich amorphous phases in their microstructure. A higher amount of amorphous phases was found in the F3S7, followed by the F4S6 and then the F5S5 sample. It should be noted that the unreacted FA was rarely found on F3S7 while it was easier to be spotted on the F5S5 sample. The existence of rich amorphous phases on the F3S7, F4S6, and F5S5 samples would be due to the rapid reaction of GGBFS in these mortars, quickly generating the hydration products, which is mainly C-(A)-S-H. It then densified the matrix of the mortars, resulting in low porosity in the specimen. Consequently, the F3S7, F4S6, and F5S5 samples revealed a high strength and low water absorption.

Noticeably, the microcracks were easily observed on the F3S7, F4S6, and F5S5, as seen in Fig. 10(b), Fig. 10(c), and Fig. 10(d), respectively. These cracks can either cross the amorphous phases/ the reaction products on the FA particles. This is in line with previous studies [24, 25] which figured out that microcracks grew in the AAFS and the micro-cracking developed over time. An adequate replacement of FA can help AAS materials to fill these microcracks and lessen the capillary pores in the mortar, resulting in high strength and low water absorption. Based on the obtained results and the SEM images of the AAFS mortar at 28 days, it is suggested that the optimum quantity of FA in the mixture should be about 40%. With that quantity, the GGBFS content in the mixture is adequate to gain significant strength while FA can help to

reduce the microcracking during the hydration process of GGBFS.

4. Conclusion

This study experimentally evaluates the engineering properties of the AAFS mortars through the tests of flowability, fresh UW, flexural and compressive strengths, water absorption, and especially drying shrinkage to clarify the adaption to using as structural building material replacing OPC-based materials in real practice. Moreover, the microstructures of the AAFS mortars are also characterized using SEM analyses. Based on the results obtained from the experiments, the following conclusions are particularly noteworthy:

1. Lower flowability and higher unit weight of the fresh AAFS mixtures are found when higher portions of GGBFS are incorporated in the mixtures. The flow diameter and fresh UW of all mortar mixtures are in the respective range of 180 – 240 mm and 2222 – 2262 kg/m³.

2. The GGBFS-rich AAFS (i.e., F3S7 and F4S6 mixtures) develops flexural and compressive strengths faster than the FA-rich AAFS. Notably, after 1 day of casting, the GGBFS-rich AAFS gains both significantly higher flexural and compressive strengths than those of the control mortar. In addition, after 7 days, all of the AAFS mortars exhibit higher mechanical strengths than the control sample, confirming the potential applicability of AAFS as being a structural material and its potential to replace OPC in the production of OPC-free mortar.

3. All of the AAFS mortars register water absorption rates in the range of 6.48 – 8.23%, which is about 13 – 32% lower than that of the OPC mortar. In this study, lower water absorption of the AAFS mortars is attributable to higher GGBFS content. This finding is in good agreement with the evolution in the mechanical strength of the AAFS mortars.

4. In line with some of the previous studies, the AAFS prepared in the present study also shows higher drying shrinkage than the OPC mortar. In addition, the AAFS samples incorporating higher GGBFS content exhibits less drying shrinkage than the FA-rich AAFS. However, further investigations should be conducted to understand the mechanism of drying shrinkage in AAFS samples.

5. The F4S6 is suggested as an optimal AAFS mixture as the mortar samples of this mixture exhibit superior engineering performance and microstructure than the other AAFS samples considered in this study. Moreover, the microstructure observation well supported other properties of the mortars as denser microstructure is associated with less drying shrinkage, lower water absorption, and consequently higher mechanical strength of the mortars.

References

- [1] A. Dwivedi and M. Jain, "Fly ash – Waste management and overview: A Review," *Recent Res. Sci. Technol.*, vol. 6, pp. 30-35, 2014.

- [2] N. Q. Pham and K. A. Le, "Coal fly ash in Vietnam and its application as a lightweight material," *Chem. Eng. Trans.*, vol. 83, pp. 31-36, 2021.
- [3] M. Motokura, J. Lee, I. Kutani, and H. Phoumin, "Improving emissions regulations for coal-fired power plants in ASEAN," ERIA Research Project Report, 2017.
- [4] T. Chompoorat, K. Thanawong, and S. Likitlersuang, "Swell-shrink behaviour of cement with fly ash-stabilised lakebed sediment," *Bull. Eng. Geol. Environ.*, vol. 80, pp. 2617-2628, 2021.
- [5] N. Yoobanpot, P. Jamsawang, K. Krairan, and P. Jongpradist, "Laboratory investigation of the properties of cement fly ash gravel for you as a column-supported embankment," *Constr. Build. Mater.*, vol. 257, p. 119493, 2020.
- [6] P. Jamsawang, S. Charoensil, T. Namjan, P. Jongpradist, and S. Likitlersuang, "Mechanical and microstructural properties of dredged sediments treated with cement and fly ash for use as road materials," *Road Mater. Pavement Des.*, vol. 22, pp. 2498-2522, 2020.
- [7] M. Adamu, P. Trabanpruek, P. Jongvivatsakul, S. Likitlersuang, and M. Iwanami, "Mechanical performance and optimization of high-volume fly ash concrete containing plastic wastes and graphene nanoplatelets using response surface methodology," *Constr. Build. Mater.*, vol. 308, p. 125085, 2021.
- [8] H. Alanazi, J. Hu, and Y. R. Kim, "Effect of slag, silica fume, and metakaolin on properties and performance of alkali-activated fly ash cured at ambient temperature," *Constr. Build. Mater.*, vol. 197, pp. 747-756, 2019.
- [9] A. Aboulayt, F. Souayfan, E. Roziere, R. Jaafri, A. C. E. Idrissi, R. Moussa, C. Justino, and A. Loukili, "Alkali-activated grouts based on slag-fly ash mixtures: From early-age characterization to long-term phase composition," *Constr. Build. Mater.*, vol. 260, p. 120510, 2020.
- [10] G. Fang, H. Bahrami, and M. Zhang, "Mechanisms of autogenous shrinkage of alkali-activated fly ash-slag pastes cured at ambient temperature within 24 h," *Constr. Build. Mater.*, vol. 171, pp. 377-387, 2018.
- [11] X. Y. Zhuang, L. Chen, S. Komarneni, C. H. Zhou, D. S. Tong, H. M. Yang, W. H. Yu, and H. Wang, "Fly ash-based geopolymer: Clean production, properties and applications," *J. Clean. Prod.*, vol. 125, pp. 253-267, 2016.
- [12] M. T. Junaid, O. Kayali, and A. Khennane, "Response of alkali activated low calcium fly-ash based geopolymer concrete under compressive load at elevated temperatures," *Mater. Struct.*, vol. 50, pp. 50, 2016.
- [13] G. Fang and M. Zhang, "Multiscale micromechanical analysis of alkali-activated fly ash-slag paste," *Cem. Concr. Res.*, vol. 135, p. 106141, 2020.
- [14] G. Fang, W. K. Ho, W. Tu, and M. Zhang, "Workability and mechanical properties of alkali-activated fly ash-slag concrete cured at ambient temperature," *Constr. Build. Mater.*, vol. 172, pp. 476-487, 2018.
- [15] S. Samantasinghar and S. P. Singh, "Fresh and hardened properties of fly ash-slag blended geopolymer paste and mortar," *Int. J. Concr. Struct. Mater.*, vol. 13, pp. 47, 2019.
- [16] M. Chi and R. Huang, "Binding mechanism and properties of alkali-activated fly ash/slag mortars," *Constr. Build. Mater.*, vol. 40, pp. 291-298, 2013.
- [17] N. K. Lee, J. G. Jang, and H. K. Lee, "Shrinkage characteristics of alkali-activated fly ash/slag paste and mortar at early ages," *Cem. Concr. Compos.*, vol. 53, pp. 239-248, 2014.
- [18] M. Chi, W. Yeih, J. Chang, and K. Tsou, "Compressive strength and drying shrinkage of alkali-activated fly ash/slag mortars," *Int. J. Struct. Civ. Eng. Res.*, vol. 9, pp. 161-164, 2020.
- [19] M. Torres-Carrasco, and F. Puertas, "Alkaline activation of different aluminosilicates as an alternative to Portland cement: Alkali activated cements or geopolymers," *Rev. Ing. Constr.*, vol. 32, pp. 05-12, 2017.
- [20] M. J. A. Mijarsh, M. A. M. Johari, B. H. A. Bakar, Z. A. Ahmad, and A. M. Zeyad, "Influence of SiO₂, Al₂O₃, CaO, and Na₂O on the elevated temperature performance of alkali-activated treated palm oil fuel ash-based mortar," *Struct. Concr.*, vol. 22, pp. E380-E399, 2021.
- [21] T. P. Huynh, T. B. Pham, T. K. Lam, T. D. Tran, and V. T. Nguyen, "Feasibility of producing artificial aggregates by alkaline activation of fly ash-slag blends," in *2020 Applying New Technology in Green Buildings (ATiGB)*, 2021, pp. 1-5.
- [22] C. L. Hwang, D. H. Vo, and T. P. Huynh, "Physical-microstructural evaluation and sulfate resistance of no-cement mortar developed from a ternary binder of industrial by-products," *Environ. Prog. Sustain. Energy*, vol. 39, p. e13421, 2021.
- [23] X. Ouyang, Y. Ma, Z. Liu, J. Liang, and G. Ye, "Effect of the sodium silicate modulus and slag content on fresh and hardened properties of alkali-activated fly ash/slag," *Minerals*, vol. 10, p. 15, 2020.
- [24] S. Y. Oderji, B. Chen, M. R. Ahmad, and S. F. A. Shah, "Fresh and hardened properties of one-part fly ash-based geopolymer binders cured at room temperature: Effect of slag and alkali activators," *J. Clean. Prod.*, vol. 225, pp. 1-10, 2019.
- [25] F. Collins and J. G. Sanjayan, "Microcracking and strength development of alkali activated slag concrete," *Cem. Concr. Compos.*, vol. 23, pp. 345-352, 2001.
- [26] I. Wilińska, B. Pacewska, and A. Ostrowski, "Investigation of different ways of activation of fly ash-cement mixtures," *J. Therm. Anal. Calorim.*, vol. 138, pp. 4203-4213, 2019.
- [27] Y. Luo, S. H. Li, K. M. Klima, H. J. H. Brouwers, and Q. Yu, "Degradation mechanism of hybrid fly ash/slag based geopolymers exposed to elevated

- temperatures,” *Cem. Concr. Res.*, vol. 151, p. 106649, 2022.
- [28] J. Qiu, Y. Zhao, J. Xing, and X. Sun, “Fly ash/blast furnace slag-based geopolymer as a potential binder for mine backfilling: Effect of binder type and activator concentration,” *Adv. Mater. Sci. Eng.*, vol. 2019, p. e2028109, 2019.
- [29] Z. Lafhaj, M. Goueygou, A. Djerbi, and M. Kaczmarek, “Correlation between porosity, permeability and ultrasonic parameters of mortar with variable water/cement ratio and water content,” *Cem. Concr. Res.*, vol. 36, pp. 625-633, 2006.
- [30] W. T. Kuo, Y. S. Gao, and C. U. Juang, “Influence of BOF and GGBFS based alkali activated materials on the properties of porous concrete,” *Materials*, vol. 12, pp. 2214, 2019.
- [31] O. A. Mohamed, “A review of durability and strength characteristics of alkali-activated slag concrete,” *Materials*, vol. 12, pp. 1198, 2019.
- [32] A. Wardhono, D. W. Law, and T. C. K. Molyneaux, “Long term performance of alkali activated slag concrete,” *J. Adv. Concr. Technol.*, vol. 13, pp. 187-192, 2015.
- [33] F. Matalkah, T. Salem, M. Shaafaey, and P. Soroushian, “Drying shrinkage of alkali activated binders cured at room temperature,” *Constr. Build. Mater.*, vol. 201, pp. 563-570, 2019.
- [34] M. Palacios and F. Puertas, “Effect of shrinkage-reducing admixtures on the properties of alkali-activated slag mortars and pastes,” *Cem. Concr. Res.*, vol. 37, pp. 691-702, 2007.
- [35] M. Chi, “Effects of dosage of alkali-activated solution and curing conditions on the properties and durability of alkali-activated slag concrete,” *Constr. Build. Mater.*, vol. 35, pp. 240-245, 2012.
- [36] R. J. Thomas, D. Lezama, and S. Peethamparan, “On drying shrinkage in alkali-activated concrete: Improving dimensional stability by aging or heat-curing,” *Cem. Concr. Res.*, vol. 91, pp. 13-23, 2017.
- [37] T. Yang, H. Zhu, and Z. Zhang, “Influence of fly ash on the pore structure and shrinkage characteristics of metakaolin-based geopolymer pastes and mortars,” *Constr. Build. Mater.*, vol. 153, pp. 284-293, 2017.
- [38] G. Wang, and Y. Ma, “Drying shrinkage of alkali-activated fly ash/slag blended system,” *J. Sustain. Cem.-Based Mater.*, vol. 7, pp. 203-213, 2018.
- [39] B. Walkley, R. S. Nicolas, M. A. Sani, G. J. Rees, J. V. Hanna, J. S. J. van Deventer, and J. L. Provis, “Phase evolution of C-(N)-A-S-H/N-A-S-H gel blends investigated via alkali-activation of synthetic calcium aluminosilicate precursors,” *Cem. Concr. Res.*, vol. 89, pp. 120-135, 2016.
- [40] I. Ismail, S. A. Bernal, J. L. Provis, R. S. Nicolas, S. Hamdan, and J. S. J. van Deventer, “Modification of phase evolution in alkali-activated blast furnace slag by the incorporation of fly ash,” *Cem. Concr. Compos.*, vol. 45, pp. 125-135, 2014.



Hai Yen Thi Nguyen was born in Binh Thuan, Vietnam. She received the B.S. degree in Construction Material Engineering from the Ho Chi Minh City University of Technology in 2011 and the M.S. in Structural Engineering from Chulalongkorn, Thai Lan in 2013. She completed her Ph.D. in the Division of Engineering and Policy for Sustainable Environment at Hokkaido University, Japan in 2016.

From Dec 2016 to April 2019, she was a postdoctoral researcher at National Institute for Materials Science, Japan. Since 2019, she has been a lecturer at the Faculty of Civil Engineering, Industrial University of Ho Chi Minh City. Her research interests include the microstructure of cement and concrete, geopolymers, alkaline-activated materials, and the durability of materials.



Nguyen Thi Cao was born in My Tho city, Tien Giang province, Vietnam. He received the B.S. and M.S. degrees in Construction Materials Engineering from the Ho Chi Minh City University of Technology, Ho Chi Minh City, Vietnam in 2011 and 2013 and the Ph.D. degree in Civil Engineering from Chulalongkorn University, Bangkok, Thailand in 2017.

Since 2011, he has been a lecturer at the Department of Civil Engineering, Faculty of Engineering, Tien Giang University. His research interests include advanced concrete technology, green materials, FRP materials. He is an Associate Editor in the Journal of Science - Tien Giang University.



Tran Dong Minh Ngoc was born in Can Tho city, Vietnam. She received the B.S. degree in Civil Engineering and the M.S. degree in Hydraulic Engineering from Can Tho University, Vietnam in 2003 and 2021, respectively.

Her current interests include green concrete, alkali-activated materials, and the application of cementitious materials in concrete.



Trong-Phuoc Huynh was born in An Giang province, Vietnam. He received the B.S. degree in Civil Engineering from Can Tho University, Vietnam in 2010 and the M.S. and Ph.D. degrees in Civil Engineering (Construction Materials) from National Taiwan University of Science and Technology, Taiwan in 2013 and 2016, respectively.

He is currently working at the Department of Civil Engineering, Can Tho University, Vietnam as a lecturer. He is the author/co-author of over 70 scientific publications and two international patents. His current interests include concrete science and technology; green and advanced building materials; alkali-activated materials and geopolymers; application of pozzolanic materials; turning wastes into construction materials.